Aggregate Morphologies of Amphiphilic Graft Copolymers in Dilute Solution Studied by Self-Consistent Field Theory

Liangshun Zhang, Jiaping Lin,* and Shaoliang Lin

Key Laboratory for Ultrafine Materials of Ministry of Education, School of Materials Science and Engineering, East China University of Science and Technology, Shanghai 200237, China

Received: December 7, 2006; In Final Form: March 30, 2007

Microstructures assembled by amphiphilic graft copolymers in a selective solvent (poor for the backbone chain and good for graft chains or poor for graft chains and good for the backbone chain) were investigated on the basis of a real-space algorithm of self-consistent field theory in two-dimensions. Circle-like micelles, line-like micelles, large compound micelles, and vesicles are obtained by tailoring the architectural parameters and interaction parameter between the graft blocks and solvents. The aggregate morphology stability regions of graft copolymers as functions of the position of first graft point and the number of branches are constructed. It is found that the architectural parameters play a remarkable role in the complex microstructure formation. The interaction between the graft blocks and solvents is also shown to exert an effect on the morphology stability regions. The distributions of the free end and inner blocks of the backbone are found to be different in various aggregate structures. For the circle-like micelles assembled by graft copolymers with a hydrophobic backbone and vesicles assembled by graft copolymers with a hydrophilic backbone, the free end and inner blocks segregate and localize in different parts of the aggregates depending on their length. However, with respect to the large compound micelles and vesicles assembled by graft copolymers with a hydrophobic backbone, the free end and inner blocks uniformly mix in the clusters.

Introduction

Amphiphilic copolymers are capable of self-assembly into nanoscale structures in solution, in bulk, and at an interface. A typical example is the amphiphilic block copolymers that can associate to form complex microstructures, such as rod-like micelles, sphere-like micelles, and vesicles in selective solvents. These microstructures have attracted widespread interests in both a fundamental and a technological context, as they can be used in the fields of delivery and release of drugs, agrochemisty, personal care, and food products.[1,2] So far, most work on aggregation behavior of amphiphilic copolymers focuses on linear molecular architectures. With the development of new synthetic methods, the aggregation behavior of well-defined copolymers with more complex architectures such as graft, starblock, and miktoarm copolymers has been studied experimentally.[3−15] Among these well-defined copolymers, much attention has been paid to aggregates formed by amphiphilic graft copolymers owing to their sensitivity to the external chemical and physical stimuli such as temperature, pH, ionic strength, solvent composition, electric field, and light.[16−22] Regarding the diverse applications, it is important to control the shapes and sizes of aggregate morphologies of graft copolymers by varying architectural parameters, amphiphilic properties of the backbone, preparation procedures, and so on.

In contrast to the situation accompanying linear diblock and triblock copolymers, there has been much less theoretical research regarding the self-assembly behavior of the graft copolymers in dilute solution. Borisov et al. used the scaling theory to study aggregate morphologies of graft copolymers with a hydrophobic backbone in dilute solution.[23] They demonstrated that the pearl necklace micelles were formed at dense grafting. In the case of spare grafting, the formation of spherical and cylindrical micelles and lamellar mesophases was predicted. Kim et al. investigated the micellization for various types of π-shaped copolymers in selective solvents by using the Brownian dynamics simulation and explained the architectural effect on the micellization by mean field theory.[24] However, systematical theoretical studies on the aggregate morphologies of amphiphilic graft copolymers in dilute solution are still limited.

The self-consistent field theory (SCFT) has emerged as a powerful tool to characterize the equilibrium thermodynamical features of multiblock copolymers,[25−28] a blend of block copolymers,[29−31] rod−coil copolymers,[32,33] a mixture of diblock copolymers and naoparticles,[34−36] copolymers with complex architectures,[37−40] etc. Although SCFT has been very successful in studying the copolymers in the bulk state, the application of SCFT to the problem of self-assembled complex microstructures in dilute copolymer solution is still in its infancy. Recently, Fredrickson and co-workers suggested a new combinatorial screening method,[26, 41−43] which involved a direct implementation of SCFT in real space. For the study of the complex microstructures, a prior assumption about the morphology is not necessary. This method is found to be a useful way to study the self-assembly behavior of amphiphilic copolymers in dilute solution. Liang and co-workers applied the Fredrickson's method to investigate the formation of the microstructures assembled by the linear block copolymers in dilute solution in two-dimensional space.[44, 45] Complex micelles (e.g., sphere-like micelles and rod-like micelles) and vesicles were obtained by tailoring the interaction parameters, initial density fluctuation, and polydispersity. Wang et al. employed the same method to investigate the aggregate morphologies of amphiphilic **ABC** triblock copolymers in dilute solution by changing the hydro-

* Corresponding author. Tel: +86-21-64253370. Fax: +86-21-64253539. E-mail address: jplinlab@online.sh.cn.

10.1021/jp068429l CCC: $37.00
Published on Web 07/17/2007

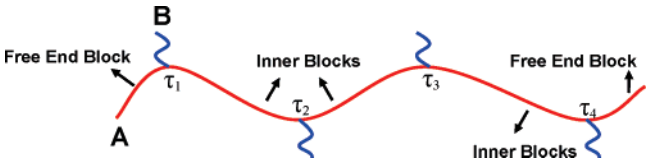

Figure 1. Molecular architecture of the graft copolymer.

phobic degree between the blocks **B** and **C**.[46] Peanut-like micelles not observed for diblock copolymers and large compound micelles due to macrophase separation were found. Li et al. studied the effect of polydispersity on block copolymer self-assembly.[47] The morphological transition from vesicles to micelles was observed when the polydispersity of copolymers was increased. Although these theoretical studies reproduce the general features of experimentally observed microstructures, more models are still needed in order to elucidate the effect of a complex molecular architecture on the self-assembly behavior of amphiphilic graft copolymers.

In this paper, we use a combination screening method based on the real-space implementation of the SCFT, developed by Fredrickson's group,[26,41−43] to study the equilibrium microstructures assembled by graft copolymers in dilute solution in two-dimensional space. As far as we know, the self-assembly behavior of graft copolymers in dilute solution has not yet been studied by SCFT. The graft copolymer as schematically represented in Figure 1 exhibits two distinctive architectural parameters: the number of branches (m) and the graft point position (τ_i), which determine the structure of the graft copolymer.[48] In addition to examining the impact of m and τ_i on the aggregation behavior, we also studied the effect of the interaction between the graft blocks and solvents on the microstructures of graft copolymer aggregates. It was demonstrated that m and τ_i are two important parameters in determining the microstructures assembled by the graft copolymers. The formed aggregate morphologies are also affected by the interaction between the graft blocks and solvents.

In this work, the SCFT calculation was only performed in 2D because solving the SCFT equations in 3D real space still has some computational and time challenge. The circle-like micelles and line-like micelles in 2D could correspond to sphere-like micelles and rod-like micelles in 3D, respectively. More complex aggregate morphologies may appear in 3D. This causes the aggregate morphology stability regions to have some alterations. However, the 2D calculation is able to catch the essential features, such as the effect of architecture parameters on the self-assembly behavior of graft copolymers, the order of the morphological transition, the structures of aggregates, and the density distributions of blocks in the cluster. The obtained results are useful for understanding the mechanism for the aggregate morphologies of graft copolymers in dilute solution, including vesicles, circle-like micelles, and line-like micelles.

Self-Consistent Field Theory for Graft Architecture

We consider a system with volume V, containing n_G graft copolymers and n_S solvent molecules **S**. As shown in Figure 1, each copolymer is comprised of a flexible homopolymer **A** backbone along which m flexible homopolymer **B** grafts are spaced. The degrees of polymerization of the **A** and **B** chains are N_A and N_B, respectively. f_A and f_B denote the volume fractions of **A**-type and **B**-type monomers of each copolymer chain, respectively. The volume fraction of graft copolymers in solution is f_G and that of solvents is $f_S = 1 - f_G$. The ith graft is located at τ_i given by

$$\tau_i = \tau_1 + \frac{(i-1)(1-2\tau_1)}{m-1} \qquad 1 \le i \le m \tag{1}$$

Within this mean-field theory the configurations of single copolymer chain and solvent are determined by a set of effective chemical potential fields $w_K(\mathbf{r})$ ($K = A, B, S$), replacing actual interactions within the solution. These potential fields are conjugated to the density fields $\varphi_K(\mathbf{r})$. We invoke an incompressibility [$\varphi_A(\mathbf{r}) + \varphi_B(\mathbf{r}) + \varphi_S(\mathbf{r}) = 1$] by introducing a Lagrange multiplier $\xi(\mathbf{r})$. For such a graft copolymer solution, the free energy (in units of k_BT) is given by

$$F = -f_G \ln\frac{Q_G}{V} - f_S N_G \ln\frac{Q_S}{V} - \frac{1}{V}\int d\mathbf{r}\,[w_A(\mathbf{r})\,\varphi_A(\mathbf{r}) + w_B(\mathbf{r})\,\varphi_B(\mathbf{r}) + w_S(\mathbf{r})\,\varphi_S(\mathbf{r}) - \chi_{AB}N_G\varphi_A(\mathbf{r})\,\varphi_B(\mathbf{r}) - \chi_{AS}N_G\varphi_A(\mathbf{r})\,\varphi_S(\mathbf{r}) - \chi_{BS}N_G\varphi_B(\mathbf{r})\,\varphi_S(\mathbf{r}) + \xi(\mathbf{r})(1 - \varphi_A(\mathbf{r}) - \varphi_B(\mathbf{r}) - \varphi_S(\mathbf{r}))] \tag{2}$$

In this expression, the Flory−Huggins parameters χ_{IJ} characterize the interactions between species I and J, and $N_G = N_A + mN_B$ denotes the total degree of polymerization of graft copolymer. Q_S is the partition function for a solvent in the field $w_S(\mathbf{r})$ given by

$$Q_S = \int d\mathbf{r} \exp\left(-\frac{w_S(\mathbf{r})}{N_G}\right) \tag{3}$$

$Q_G = \int d\mathbf{r}\; q_A(\mathbf{r},1)$ is the partition function for a single noninteracting, grafted chain subject to the fields $w_A(\mathbf{r})$ and $w_B(\mathbf{r})$ in terms of backbone propagator $q_A(\mathbf{r},s)$.The contour length s increases continuously from 0 to 1 as the block changes from one end of the homopolymer chain to the other. The spatial coordinate $\mathbf{r}$ is in units of R_g, where $R_g^2 = N_G a^2/6$ (a is the statistical segment length).

The backbone propagator is divided into $m + 1$ segments

$$q_A(\mathbf{r},s) = q_A^{(j)}(\mathbf{r},s)$$

$$\text{for } \tau_j \le s < \tau_{j+1} \qquad j = 0,1,\cdots, m$$

$$\tau_0 \equiv 0 \quad \tau_{m+1} \equiv 1 \tag{4}$$

where each segment satisfies the modified diffusion equation

$$\frac{N_G}{N_A}\frac{\partial q_A^{(j)}(\mathbf{r},s)}{\partial s} = \nabla^2 q_A^{(j)}(\mathbf{r},s) - w_A(\mathbf{r})\,q_A^{(j)}(\mathbf{r},s) \tag{5}$$

and is subject to the following initial conditions:

$$q_A^{(j)}(\mathbf{r},\tau_j) = q_A^{(j-1)}(\mathbf{r},\tau_j)\,q_B(\mathbf{r},1) \qquad j = 1, 2, ..., m$$

$$q_A^{(0)}(\mathbf{r},0) = 1 \tag{6}$$

Here, $q_B(\mathbf{r},s)$ is a propagator for **B** graft that satisfies the following modified diffusion equation:

$$\frac{N_G}{N_B}\frac{\partial q_B(\mathbf{r},s)}{\partial s} = \nabla^2 q_B(\mathbf{r},s) - w_B(\mathbf{r})\,q_B(\mathbf{r},s) \qquad 0 \le s \le 1 \tag{7}$$

and is subject to the initial condition $q_B(\mathbf{r},0) = 1$ for the free end of the graft at $s = 0$. We also define a back-propagator of the jth **B** chain, $q_{Bj}^{+}(\mathbf{r},s)$. It satisfies eq 7 and starts on the end

of the **B** chain tethered to the backbone. It is therefore subject to the initial condition

$$q_{\mathrm{B}j}^{+}(\mathbf{r},0) = \frac{q_{\mathrm{A}}^{(j)}(\mathbf{r},\tau_j)\, q_{\mathrm{A}}^{(m+1-j)}(1-\tau_j)}{q_{\mathrm{B}}{}^{2}(\mathbf{r},1)} \tag{8}$$

In terms of these propagators, the densities are given by

$$\varphi_{\mathrm{A}}(\mathbf{r}) = \sum_{i=1}^{m+1} \varphi_{\mathrm{A}}^{i}(\mathbf{r}) = \frac{Vf_{\mathrm{G}}f_{\mathrm{A}}}{Q_{\mathrm{G}}} \sum_{i=1}^{m+1} \int_{\tau_{i-1}}^{\tau_i} \mathrm{d}s\, q_{\mathrm{A}}(\mathbf{r},s)\, q_{\mathrm{A}}(\mathbf{r},1-s) \tag{9}$$

$$\varphi_{\mathrm{B}}(\mathbf{r}) = \frac{Vf_{\mathrm{G}}f_{\mathrm{B}}}{mQ_{\mathrm{G}}} \sum_{j=1}^{m} \int_{0}^{1} \mathrm{d}s\, q_{\mathrm{B}}(\mathbf{r},s) q_{\mathrm{B}j}^{+}(\mathbf{r},1-s) \tag{10}$$

$$\varphi_{\mathrm{S}}(\mathbf{r}) = \frac{Vf_{\mathrm{S}}}{Q_{\mathrm{S}}} \exp\left[-\frac{w_{\mathrm{S}}(\mathbf{r})}{N_{\mathrm{G}}}\right] \tag{11}$$

where $\varphi_A^i(\mathbf{r})$ is the density of backbone blocks between τ_{i-1} and τ_i. Finally, the minimization of the free energy F with respect to $\varphi_{\mathrm{A}}(\mathbf{r})$, $\varphi_{\mathrm{B}}(\mathbf{r})$, $\varphi_{\mathrm{S}}(\mathbf{r})$, and $\xi(\mathbf{r})$ leads to the set of mean-field equations

$$w_{\mathrm{A}}(\mathbf{r}) = \chi_{\mathrm{AB}}N_{\mathrm{G}}\varphi_{\mathrm{B}}(\mathbf{r}) + \chi_{\mathrm{AS}}N_{\mathrm{G}}\varphi_{\mathrm{S}}(\mathbf{r}) + \xi(\mathbf{r}) \tag{12}$$

$$w_{\mathrm{B}}(\mathbf{r}) = \chi_{\mathrm{AB}}N_{\mathrm{G}}\varphi_{\mathrm{A}}(\mathbf{r}) + \chi_{\mathrm{BS}}N_{\mathrm{G}}\varphi_{\mathrm{S}}(\mathbf{r}) + \xi(\mathbf{r}) \tag{13}$$

$$w_{\mathrm{S}}(\mathbf{r}) = \chi_{\mathrm{AS}}N_{\mathrm{G}}\varphi_{\mathrm{A}}(\mathbf{r}) + \chi_{\mathrm{BS}}N_{\mathrm{G}}\varphi_{\mathrm{B}}(\mathbf{r}) + \xi(\mathbf{r}) \tag{14}$$

$$\varphi_{\mathrm{A}}(\mathbf{r}) + \varphi_{\mathrm{B}}(\mathbf{r}) + \varphi_{\mathrm{S}}(\mathbf{r}) = 1 \tag{15}$$

To solve the SCFT equations, we use a variant of the algorithm developed by Fredrickson and co-workers.[26,41−43] The initial values of the fields $w_J(\mathbf{r})$ are constructed by $w_J(\mathbf{r}) = \sum_{I\neq J}\chi_{IJ}N_{\mathrm{G}}\varphi_I(\mathbf{r})$, where $\varphi_I(\mathbf{r})$ satisfies the Gaussian distributions[44]

$$\langle \varphi_I(\mathbf{r}) - c_I \rangle = 0 \tag{16}$$

$$\langle (\varphi_I(\mathbf{r}) - c_I)(\varphi_J(\mathbf{r}') - c_J) \rangle = \beta c_I c_J \delta_{IJ} \delta(\mathbf{r} - \mathbf{r}') \tag{17}$$

Here, β characterizes the amplitude of initial density fluctuation, c_I (I = A, B, and S) are the volume fractions of block **A**, block **B**, and solvent **S** in solution, respectively. The diffusion equations are solved with the Baker-Hausdorff operator splitting formula proposed by Rasmussen et al.,[49, 50] which has higher stability and accuracy than other methods for the same spatial discretization. For example, the diffusion equation, eq 5, is discretized according to

$$q_{\mathrm{A}}^{(j)}(\mathbf{r}, s+ds) = \exp\left[-\frac{ds\, f_{\mathrm{A}}}{2} w_{\mathrm{A}}(\mathbf{r})\right] \exp[ds f_{\mathrm{A}} \nabla^2] \times \exp\left[-\frac{ds\, f_{\mathrm{A}}}{2} w_{\mathrm{A}}(\mathbf{r})\right] q_{\mathrm{A}}^{(j)}(\mathbf{r},s) + O(ds^3) \tag{18}$$

The operator $\exp[-ds f_{\mathrm{A}} w_{\mathrm{A}}(\mathbf{r})/2]$ is trivially implemented, whereas the operator $\exp[-ds f_{\mathrm{A}} \nabla^2]$ is implemented exactly in Fourier transform domain of the spatial variable. A fast Fourier transformation (FFTW) package is applied in the evaluation of the diffusion operator to ensure precision and convergence.[51] The procedure of solving eq 7 is similar to that of eq 5. Next, the right-hand sides of eqs 9−11 are evaluated to obtain new expression values for the volume fractions $\varphi_I(\mathbf{r})$ of species I. To ensure the incompressibility of the system, the effective pressure field $\xi(\mathbf{r})$ is obtained through solving eqs 12−15.[44] Finally, the potential fields $w_I(\mathbf{r})$ and pressure filed $\xi(\mathbf{r})$ are updated using eqs 12−14 by means of a two-step Anderson mixing scheme.[52] The numerical simulation is carried out until the relative free energy changes at each iteration are smaller than 10^{-5} and the incompressibility condition is achieved.

All simulations were done in two dimensions on a 128 × 128 lattice with periodic boundary conditions. Contours step size was set as 0.01. Adjusting the box size was used to minimize the free energy, as suggested by Bohbot-Raviv and Wang.[53] The box size corresponding to the lowest free energy upon convergence was chosen as the most appropriate one. It is noted that the resulting aggregate morphologies depend on the amplitude of initial density fluctuation. As a result, the same initial density fluctuation amplitude ($\beta = 10^{-3}$) was used in our simulations to ensure that the obtained morphologies were not affected by the initial fluctuation as it was done for the self-assembly of copolymers in dilute solution in literatures.[44−47] Following Fredrickson's method of real space implementation of SCFT, [26, 41−43] which is found to be an efficient way to tackle the problem of self-assembled complex structures in dilute copolymer solution,[44−47] we started from a Gaussian distribution initial density profile and let the system evolve to equilibrium in 2D lattice space. To check the dependence of the obtained structure on the initial state, the different random numbers were used to generate the Gaussian distributions at a given initial density fluctuation amplitude.[26,43] In the calculations, the simulations starting from a homogeneous copolymer solution were repeated 10−20 times using different initial random states and different random numbers to ensure that the observed phenomena are not accidental.

Results and Discussion

The volume fraction of graft copolymers in solution is set as $f_{\mathrm{G}} = 0.10$ in our work.[54] The polymerization degree of the graft copolymer N_{G} is assumed to have a value of 28, and the hydrophobic part composition of the graft copolymer is taken to be 0.75 in all simulations. The initial density fluctuation amplitude β is set to be 10^{-3} according to ref 44. With the constraint of eq 1, the graft points τ_i can be only determined by the position of the first junction τ_1. In terms of the solubility of the main chain and side chains, the SCFT studies reported below were carried out for two cases. One is that the backbone is hydrophobic and the grafts are hydrophilic. The other scenario is that the solvent is preferential to main chain and poor to side chains. In this paper, we focus on the phase behavior and aggregate morphologies of amphiphilic graft copolymers in dilute solution for architectural parameters, such as the position of the first graft point and the number of branches, and the interaction between the graft blocks and solvents.

A. Amphiphilic Graft Copolymers with Hydrophobic Backbone. In this subsection, the effects of architectural parameters and the interaction between the graft blocks and solvents were investigated. As for the graft copolymers with hydrophobic backbone and hydrophilic grafts, the interaction parameter $\chi_{\mathrm{AB}}N_{\mathrm{G}}$ between the incompatible blocks **A** and **B** is set as 48.0, because we are only concerned that the value should be sufficiently large to drive the microphase separation of the blocks. To model the affinity between the solvents and one of the blocks (**B**) and investigate the effect of solvent quality on the self-assembly behavior, the interaction parameter $\chi_{\mathrm{BS}}N_{\mathrm{G}}$ is set as −15.0 or −22.0. With respect to the interaction parameter

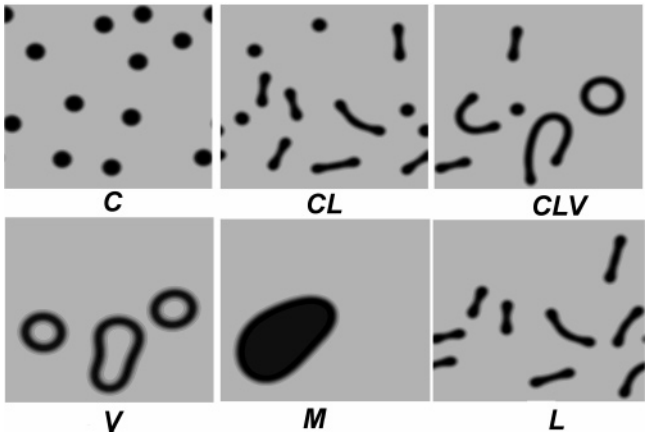

Figure 2. Density plots of the aggregate morphologies formed by graft copolymers with hydrophobic backbone in dilute solution. The colors range from light gray(**S**-rich region) to black (**A**-rich regions). Notation: ***C*** (circle-like micelles), ***CL*** (mixture of circle-like and line-like micelles), ***CLV*** (mixture of circle-like, line-like, and vesicle aggregates), ***V*** (vesicles), ***M*** (large compound micelles), and ***L*** (line-like micelles).

$\chi_{AS}N_G$, a value of 50.0 is adopted. This makes the solvents tend to be excluded from the **A** domains. All kinds of morphologies obtained for graft copolymers in dilute solution under the present conditions are shown in Figure 2. The morphologies are represented with different colors, corresponding to the intensity of local composition. The colors range from light gray (**S**-rich region) to black (**A**-rich regions). We use the notation ***C*** for circle-like micelles, ***L*** for line-like micelles, ***V*** for vesicles, ***M*** for large compound micelles, ***CL*** for a mixture containing circle-like and line-like micelles, and ***CLV*** for a mixture containing circle-like, line-like, and vesicle aggregates.

The morphology stability regions as a function of the position of first graft point τ_1 for graft copolymers with various number of branches m are shown in Figure 3a. Colors indicate the stable range for each kind of morphology. For $m = 2$, only two types of aggregate morphologies (i.e., ***C*** and ***CL***) are observed. The pure circle-like micelles are produced at larger and smaller values of τ_1, whereas the line-like micelles form at an intermediate value of τ_1. For $m = 3$, transitions of ***CL*** $\rightarrow$ ***CLV*** $\rightarrow$ ***CL*** $\rightarrow$ ***C*** take place when τ_1 increases from 0.0 to 0.50. When $m = 4$, pure vesicles are observed over the range $0.09 \leq \tau_1 \leq 0.26$. As the number of branches further increases to 5, macrophase separation occurs, and a large compound micelle forms over the range $0.0 \leq \tau_1 \leq 0.30$.

From Figure 3a, the influence of the branch number m on the aggregate morphologies can also be viewed. In the region of larger τ_1, the pure circle-like micelles are observed, and the stability region becomes broader as m increases. In the region of smaller τ_1, the aggregate morphologies change from ***C*** to ***CL***, then to ***CLV***, and finally to ***M***, as m increases. In the region of intermediate τ_1, the stability region of ***CL*** becomes narrower as m increases from 2 to 4 and finally disappears when $m = 5$. When $m = 3$ and 4, the vesicles are observed in addition to the circle-like and line-like micelles.

In the present work, the studies are limited in one graft copolymer composition. We should elucidate that the morphological transitions among the vesicles, circle-like micelles, and line-like micelles may also take place when the composition of the graft copolymer changes. For example, as for the graft copolymers with hydrophobic backbone, a mixture of circle-like and line-like micelles is observed when the volume fraction of the hydrophobic backbone is 0.75 ($m = 2$, and $\tau_1 = 0.25$), as shown in Figure 3a. When the volume fraction increases to 0.87, the vesicles emerge.

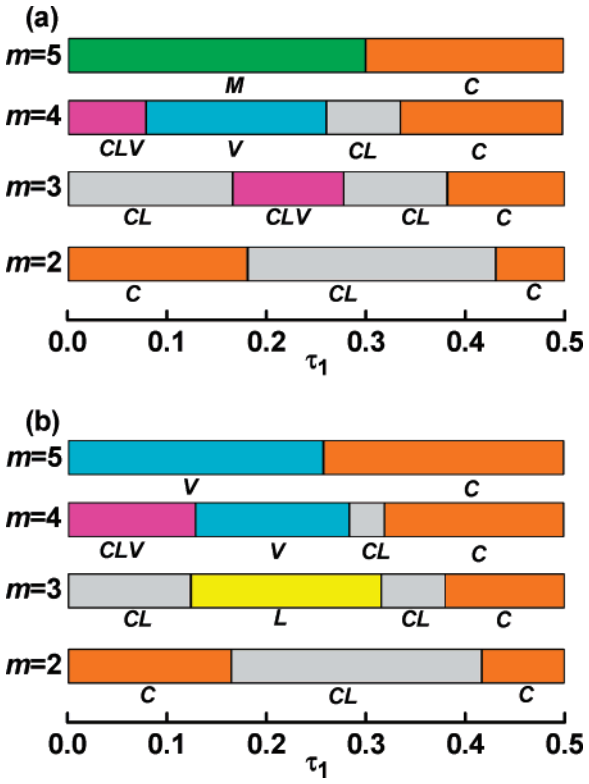

Figure 3. Aggregate morphology stability regions as a function of the position of first graft point τ_1 for graft copolymers with various number of branches m for $\beta = 10^{-3}$, $\chi_{AB}N_G = 48.0$, $\chi_{AS}N_G = 50.0$. (a) $\chi_{BS}N_G = -15.0$; (b) $\chi_{BS}N_G = -22.0$. Colors indicate the range for each kind of morphology.

The effect of the interaction parameter between the graft blocks and solvents is shown in Figure 3b where $\chi_{BS}N_G$ is set to be -22.0. As it can be seen, the morphological transition from the large compound micelles to vesicles takes place when the hydrophilicity of graft blocks is increased. It also noted that the vesicles disappear while line-like micelles form with an increase in $\chi_{BS}N_G$ when $m = 3$. The circle-like micelle stability region in the larger τ_1 becomes broader when $\chi_{BS}N_G = -22.0$.

Due to the complexity of system, we only discuss the effect of the interaction parameter between the graft blocks and solvents on the self-assembly behavior of the graft copolymers. The other interaction parameters, such as the interaction parameter between the incompatible blocks and the interaction parameter between backbone blocks and solvents, also have some effect on the self-assembly behavior of the graft copolymers. For example, when $\chi_{AS}N_G = 50.0$ ($m = 2$, and $\tau_1 = 0.33$), mixture of circle-like and line-like micelles is produced as shown in Figure 3a. When $\chi_{AS}N_G$ changes to 45.0, the graft copolymers with a hydrophobic backbone form the line-like micelles.

In order to obtain detailed information about the microstructures, the volume fractions of the free end, inner, and total backbone blocks are analyzed for the circle-like micelles (Figure 4), vesicles (Figure 5), and large compound micelles (Figure 6). The total volume fraction $\varphi_A(\mathbf{r})$, volume fractions of free end blocks $\varphi_A^1(\mathbf{r})$ and middle blocks $\varphi_A^2(\mathbf{r})$ for the circle-like micelles are shown in Figure 4. The inserts show the two-dimensional density field of backbone blocks. Figure 4a shows the typical results for $m = 2$, $\tau_1 = 0.05$, corresponding to the longer middle blocks. The shorter free end blocks distribute at the interface between the core and corona of the micelle. The longer middle blocks are predominantly concentrated in the region of cores. As τ_1 increases to 0.45, corresponding to the longer free end blocks, a different scenario

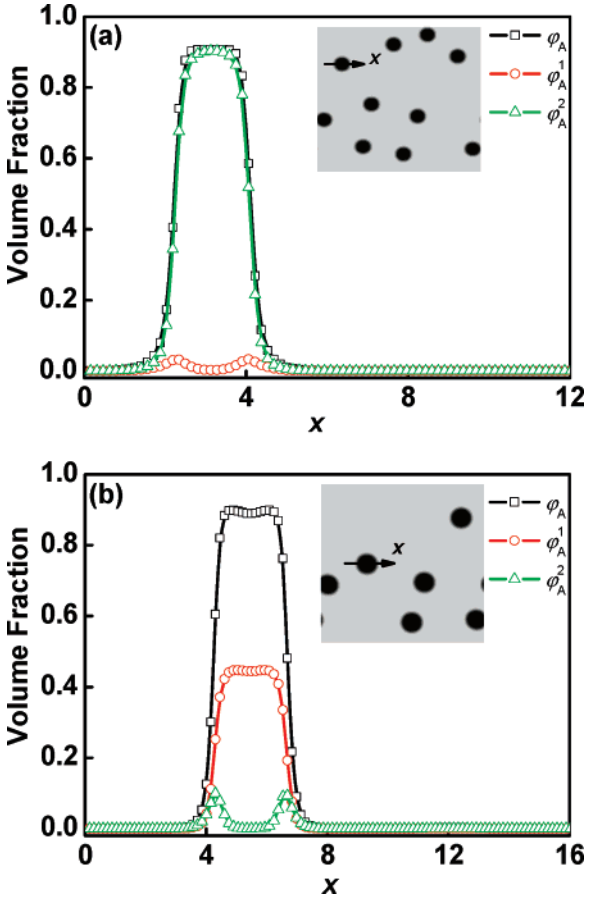

Figure 4. Profiles of the total volume fraction $\varphi_A(\mathbf{r})$ and volume fractions of blocks between τ_{i-1} and τ_i, $\varphi_A^i(\mathbf{r})$ on a cross section of the circle-like micelle marked with an arrow in the insert at $\chi_{AB}N_G = 48.0$, $\chi_{AS}N_G = 50.0$, and $\chi_{BS}N_G = -15.0$. The architectural parameters are (a) $m = 2$, $\tau_1 = 0.05$; (b) $m = 2$, $\tau_1 = 0.45$. The insert shows the two-dimensional density distribution of backbone blocks.

is observed. The longer free end blocks aggregate in the cores of circle-like micelles, as shown in Figure 4b. The shorter middle blocks are localized along the interface.

As previously described, the vesicles are produced when $m = 4$, $0.0 \le \tau_1 \le 0.26$. The profiles of the total volume fraction $\varphi_A(\mathbf{r})$ and the volume fractions contributed from the blocks between τ_{i-1} and τ_i, $\varphi_A^i(\mathbf{r})$ are shown in Figure 5. Figure 5, panels a and b, illustrates the results for $\tau_1 = 0.10$ and 0.25, respectively. The inserts show the two-dimensional density field of backbone blocks and enlarged profiles of volume fractions of inner blocks and free end blocks. The profile of $\varphi_A(\mathbf{r})$ displays a bimodal feature (i.e., the backbone blocks form the wall of the vesicle). The curves of the volume fraction of free end blocks, $\varphi_A^1(\mathbf{r})$ and $\varphi_A^5(\mathbf{r})$ are indistinguishable in the $\tau_1 = 0.10$ and 0.25 cases. It is ascribed to the fact that the architecture of graft copolymers is symmetry. Similarly, the distributions of volume fractions of inner blocks, $\varphi_A^2(\mathbf{r})$, $\varphi_A^3(\mathbf{r})$, and $\varphi_A^4(\mathbf{r})$, have the same characteristic as those of free end blocks. The peak positions of the volume fractions of inner blocks and free end blocks are identical, and density profiles are symmetric with respect to the center of the wall. These indicate that free end blocks and inner blocks are not separated. However, there are also some differences as τ_1 changes. For $\tau_1 = 0.10$, corresponding to the longer inner blocks, the wall of vesicle is predominantly concentrated by the inner blocks (Figure 5a). For $\tau_1 = 0.25$, corresponding to the shorter inner blocks, the free end blocks dominate the wall of vesicle (Figure 5b).

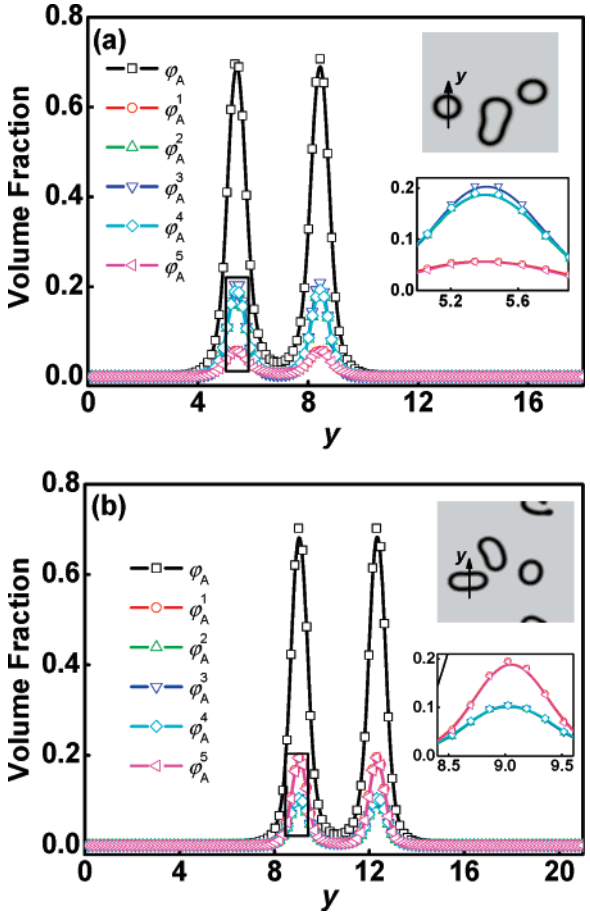

Figure 5. Profiles of the total volume fraction $\varphi_A(\mathbf{r})$ and volume fractions of blocks between τ_{i-1} and τ_i, $\varphi_A^i(\mathbf{r})$ on a cross section of the vesicle marked with an arrow in the insert at $\chi_{AB}N_G = 48.0$, $\chi_{AS}N_G = 50.0$, and $\chi_{BS}N_G = -15.0$. The architectural parameters are (a) $m = 4$, $\tau_1 = 0.10$; (b) $m = 4$, $\tau_1 = 0.25$. The inserts show the two-dimensional density distribution of backbone blocks and enlarged profiles of the volume fractions of inner blocks and free end blocks.

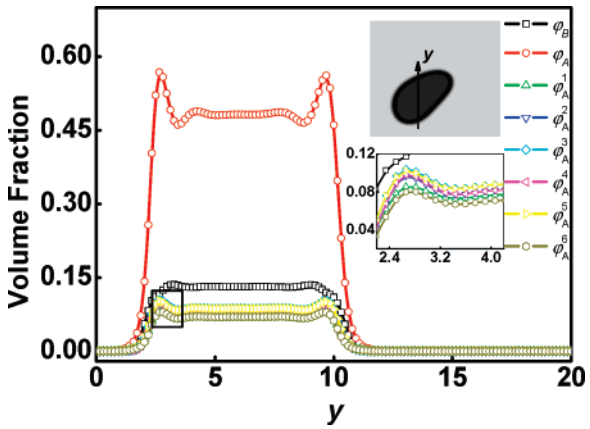

Figure 6. Profiles of the total volume fractions $\varphi_A(\mathbf{r})$, $\varphi_B(\mathbf{r})$, and volume fractions of blocks between τ_{i-1} and τ_i, $\varphi_A^i(\mathbf{r})$ on a cross section of the cluster marked with an arrow in the insert at $\chi_{AB}N_G = 48.0$, $\chi_{AS}N_G = 50.0$, and $\chi_{BS}N_G = -15.0$. The architectural parameters are $m = 5$, $\tau_1 = 0.20$. The inserts show the two-dimensional density distribution of backbone blocks and enlarged profiles of the volume fractions of inner blocks and free end blocks.

When the graft blocks have low hydrophilicity, the macrophase separation occurs and the large compound micelles form over the range $0.0 \le \tau_1 \le 0.30$ at $m = 5$. The profiles of volume fraction $\varphi_B(\mathbf{r})$, total volume fraction $\varphi_A(\mathbf{r})$, and volume fractions $\varphi_A^i(\mathbf{r})$ are illustrated in Figure 6. The density profile of

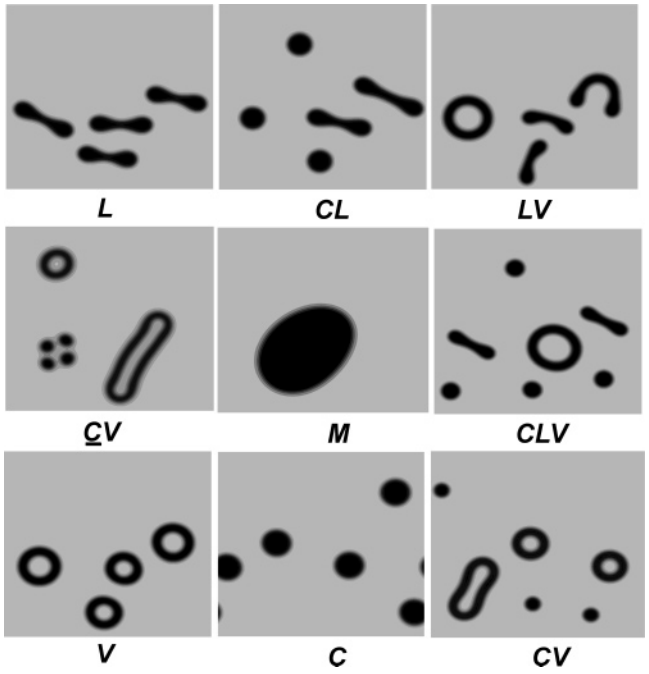

Figure 7. Density plots of the aggregate morphologies formed by graft copolymers with hydrophilic backbone in dilute solution. The colors range from light gray (**S**-rich region) to black (**B**-rich regions). In addition to the microstructures as shown in Figure 2, new morphologies, i.e., mixture of line-like and vesicle aggregates (***LV***), mixture of connected circle-like and vesicle aggregates (***CV***), and mixture of circle-like and vesicle aggregates (***CV***), emerge.

hydrophilic blocks $\varphi_B(\mathbf{r})$ has a plateau in the region rich in hydrophobic blocks. The density distribution of hydrophobic blocks $\varphi_A(\mathbf{r})$ has a quasibimodal feature similar to vesicles, with two small peaks at the interface and a plateau in the center region of the large compound micelle. From the inserts, it can be seen that the inner blocks and free end blocks are uniformly distributed in the cluster region of large compound micelle. The volume fraction of solvents in the structure is 38.0%. These indicate that the graft copolymers are in a disordered state in the microstructures. However, as the hydrophilicity of the graft blocks increases ($\chi_{BS}N_G$ changes from -15.0 to -22.0), while the other parameters remain the same, the large compound micelles change to vesicles in order to decrease the interfacial energy, as shown in Figure 3.

B. Amphiphilic Graft Copolymers with Hydrophilic Backbone. In this subsection, we consider the case of amphiphilic graft copolymers with a hydrophilic backbone. The interaction parameter $\chi_{AB}N_G$ is also set as 48.0 to ensure the separation of the blocks **A** and **B**. To study the effect of the interaction between the graft blocks and solvents on the self-assembly behavior, $\chi_{BS}N_G$ is set as 50.0 or 60.0. A value of -15.0 is adopted for $\chi_{AS}N_G$ due to the hydrophilic nature of the backbone block **A**. The volume fraction f_B of hydrophobic graft blocks of the graft copolymers is set as 0.75. The aggregate morphologies of amphiphilic graft copolymers can be tuned by molecular architecture, such as the position of grafts and the number of branches. Figure 7 shows all kinds of aggregate morphologies formed by the graft copolymers with a hydrophilic backbone. In addition to the morphologies which have been found for the graft copolymers with a hydrophobic backbone (as shown in Figure 2), new morphologies emerge. These new morphologies are as follows: a mixture of line-like and vesicle aggregates (***LV***), a mixture of connected circle-like and vesicle aggregates (***CV***), and a mixture of circle-like and vesicle aggregates (***CV***). Colors in Figure 7 represent the intensity of local composition. The colors range from light gray (**S**-rich region) to black (**B**-rich region).

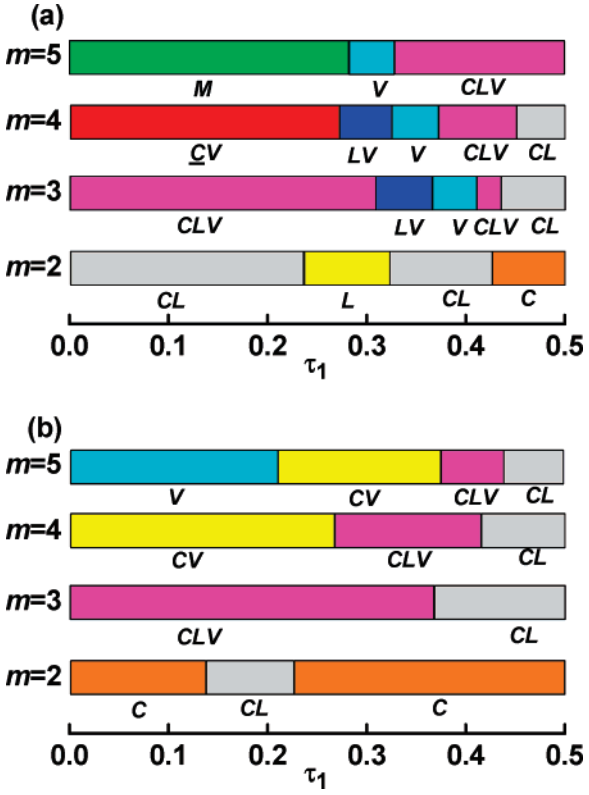

Figure 8. Aggregate morphology stability regions as a function of the position of first graft point τ_1 for graft copolymers with various number of branches m for $\beta = 10^{-3}$, $\chi_{AB}N_G = 48.0$, $\chi_{AS}N_G = -15.0$. (a) $\chi_{BS}N_G = 50.0$; (b) $\chi_{BS}N_G = 60.0$. Colors indicate the range for each kind of morphology.

Figure 8 illustrates the aggregate morphology stability regions as a function of τ_1 for graft copolymers with $m = 2-5$. Colors indicate the stability range for each kind of morphology. For $m = 2$, the pure line-like micelles are observed over the range $0.24 \le \tau_1 \le 0.32$. Out of the range, the circle-like micelles form. For $m = 3$, the vesicles appear, whereas, the stability region of pure vesicles is narrow. In the mixture of vesicles, circle-like and line-like micelles are the predominant morphology. When $m = 4$, ***CV*** is found in the smaller τ_1 region. With increasing τ_1, the transitions of ***LV*** → ***V*** → ***CLV*** → ***CL*** take place. As the number of branches further increases to 5, macrophase separation occurs, and a large compound micelle forms over the range $0 \le \tau_1 \le 0.28$.

As for the m dependence of the formed morphologies, it can also be viewed in Figure 8a. In the region of larger τ_1, as the number of branches increases, the stability regions of ***C*** and ***CL*** become narrower, and finally disappear, but the ***CLV*** region becomes broader. In the region of smaller τ_1, the aggregate morphologies change from ***CL*** to ***CLV***, then to ***CV***, and finally to ***M***, as m increases. In the region of intermediate τ_1, the type of morphologies is much more intricate than those in regions of smaller τ_1 and larger τ_1. In the region, the stability region of pure vesicles shifts to left when m increases from 3 to 5.

The effect of hydrophobicity of graft blocks on the morphology stability was further studied. For example, for $\chi_{BS}N_G = 60.0$, the morphology stability region is shown in Figure 8b. With increasing $\chi_{BS}N_G$ from 50.0 to 60.0, which means that the repulsive force between the graft blocks and solvents increases, the transitions from the large compound micelles to vesicles and the connected circle-like micelles to circle-like

micelles take place. The vesicles coexist with circle-like and line-like micelles in the intermediate τ_1 region instead of the pure vesicles at $\chi_{BS}N_G = 50.0$. At a value of larger τ_1, the stability regions of circle-like micelles and the lmixture of circle-like and line-like micelles become broader as the hydrophobicity of the graft blocks increases.

Recently, Lee et al. have experimentally examined the self-assembly behavior of poly(2-hydroxyethyl aspartamide) grafted with lactic acid oligomers (PHEA-*g*-LA) in aqueous solution.[55] In the graft copolymers, PHEA is hydrophilic, and LA is hydrophobic. The structural transition of self-aggregates as a function of DS (degree of substitution, which is the degree of grafting), corresponding to the parameter *m* in our work, was investigated. When the value of DS(*m*) is small, the aggregate shows only spherical structure. With an increase in DS(*m*), the morphology shows coexistence of spherical micelles and vesicles. A further increasing of DS(*m*) gives rise to a vesicle structure. As illustrated in Figure 8b, in a region of smaller τ_1, with an increase in *m*, the transitions ***C*** → ***CLV*** → ***CV*** → ***V*** are demonstrated. Our simulation results are qualitatively consistent with the general features of these experimental observations. So far, the experimental observations regarding the self-assembly behavior of the graft copolymers are limited, due to the unavailability of model graft copolymers with a well-defined architecture. More observations are being expected for the comparison with the simulation results.

In order to obtain more detailed information about the clusters, the volume fraction profiles of free end, inner, and total backbone blocks in vesicles (Figure 9), connected circle-like micelles (Figure 9), and large compound micelle (Figure 10) are plotted. When $m = 4$ and $\tau_1 = 0.10$, the aggregate morphology of graft copolymers shows the coexistence of the vesicles and connected circle-like micelles. The density distributions of $\varphi_A(\mathbf{r})$ and $\varphi_A^i(\mathbf{r})$ for the vesicle structure are illustrated in the right of Figure 9a. The basic building unit of the vesicle is a bilayer including inner and outer leaves. The density peaks of hydrophilic blocks in the outer leaf are lower than those in the inner leaf. Furthermore, the curves of free end blocks ($\varphi_A^1(\mathbf{r})$ and $\varphi_A^5(\mathbf{r})$) are almost indistinguishable, as shown in the inset of Figure 9a. The inner block distributions ($\varphi_A^2(\mathbf{r})$, $\varphi_A^3(\mathbf{r})$, and $\varphi_A^4(\mathbf{r})$) in the clusters are also indistinguishable like the free end block distributions. However, the shorter free end blocks tend to distribute at the interfaces between the wall and leaves. The longer inner blocks preferentially extend to the center region of the leaves. In the left of Figure 9a, the density distributions of hydrophilic blocks in the connected circle-like micelles are illustrated. One noteworthy feature is that the shells become overlapped due to the close distance between neighbor micelles, which results in a single center peak in the curve and a high volume fraction of hydrophilic blocks at the connection region. It can be seen that the shorter free end blocks distribute at the interface of the core and shell. The volume fractions of hydrophilic blocks, hydrophobic blocks, and solvents in the connection region of the connected circle-like micelles are 18.0%, 25.0%, and 57.0%, respectively. There is some degree of mixing among the hydrophilic blocks, hydrophobic blocks, and solvents in the connection region, which indicates that the repulsive force between the graft blocks and solvents is not strong. When the hydrophobicity of graft blocks increases ($\chi_{BS}N_G$ changes from 50.0 to 60.0), the connected circle-like micelles transform to single-core micelles in order to reduce the interfacial energy, as shown in Figure 8.

According to the notation proposed by Förster and co-workers, the connected circle-like micelles are called high-genus

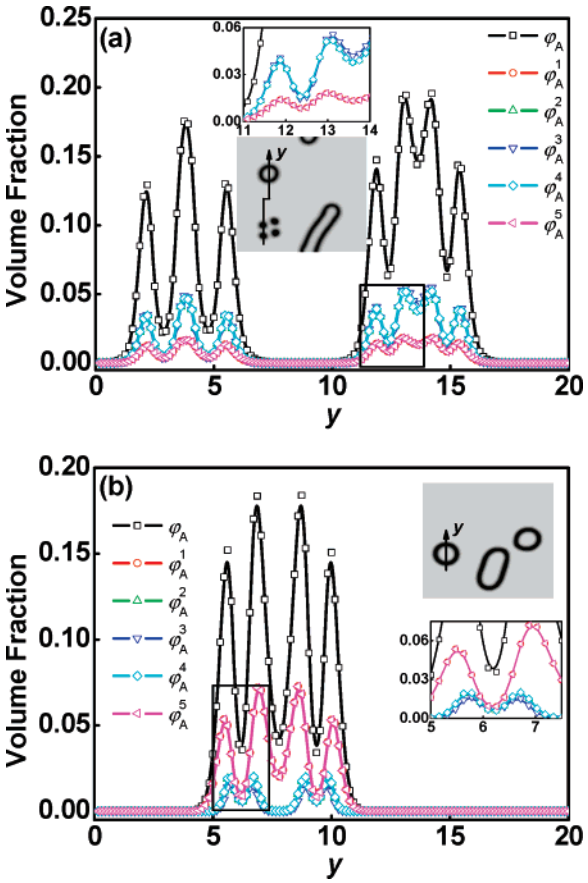

Figure 9. Profiles of the total volume fraction φ_A (**r**) and volume fractions of blocks between τ_{i-1} and τ_i, $\varphi_A^i(\mathbf{r})$ on a cross section of the clusters marked with an arrow in the insert at $\chi_{AB}N_G = 48.0$, $\chi_{AS}N_G = -15.0$, and $\chi_{BS}N_G = 50.0$. The architectural parameters are (a) $m = 4$, $\tau_1 = 0.10$; (b) $m = 4$, $\tau_1 = 0.35$. The inserts show the two-dimensional density distribution of graft blocks and enlarged profiles of the volume fractions of inner blocks and free end blocks.

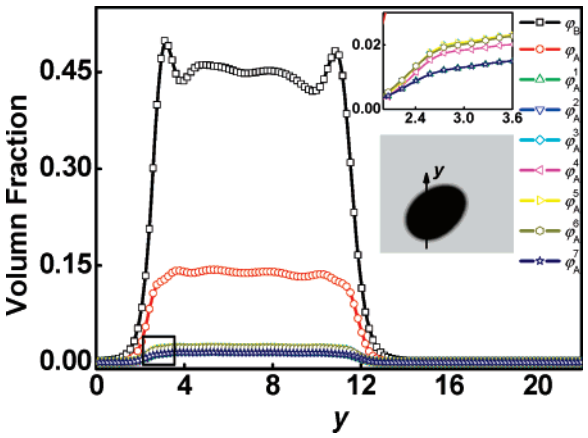

Figure 10. Profiles of the total volume fractions $\varphi_A(\mathbf{r})$, $\varphi_B(\mathbf{r})$, and volume fractions of blocks between τ_{i-1} and τ_i, $\varphi_A^i(\mathbf{r})$ on a cross section of the clusters marked with an arrow in the insert at $\chi_{AB}N_G = 48.0$, $\chi_{AS}N_G = -15.0$, and $\chi_{BS}N_G = 50.0$. The architectural parameters are $m = 6$, $\tau_1 = 0.10$. The inserts show the two-dimensional density distribution of graft blocks and enlarged profiles of the volume fractions of inner blocks and free end blocks.

nanoparticles (genus means the number of holes or handles of a particle).[56,57] Recently, some experimental evidence is available in the literature, supporting the simulation results of the connected circle-like micelles. Zhang et al. investigated the

self-assembly behavior of an amphiphilic graft copolymer with poly(*N*-isopropylacryamide) (PNIPAm) as a backbone and ethyl 4-aminobenzoate (EAB) as side chains in tetrahydrofuran (THF) solution.[58] The THF solvent is good for PNIPAm and poor for EAB. The high-genus nanoparticles were observed. The inner and outer parts of nanoparticles are composed of EAB and PNIPAm chains, respectively. Although the microstructure in our simulation has a genus of unity, the general feature that the circle-like micelles are connected is successfully reproduced.

When τ_1 increases to 0.35, the pure vesicles produce (Figure 9b). Compared with $\tau_1 = 0.10$, the vesicles become bigger and more solvents are absorbed in the center of the vesicles. The backbone blocks segregate in terms of the different length. The shorter inner blocks localize along the interfaces between the wall and leaves, and the longer free end blocks distribute in the center region of the leaves.

When the graft blocks have low hydrophobicity, the large compound micelles form over the range $0.0 \leq \tau_1 \leq 0.28$ with $m = 6$. The profiles of the volume fractions are shown in Figure 10. The volume fraction profile of hydrophobic graft blocks has two small peaks at the interface and a plateau in the center region of the cluster. The hydrophilic inner and free end blocks are uniformly distributed in the cluster. These indicate that the hydrophobic graft blocks and hydrophilic backbone blocks are almost uniformly distributed in the center region of a large compound micelle. With an increase in the hydrophobicity of graft blocks, the large compound micelle transforms to the vesicles in order to decrease the interfacial energy between the graft blocks and solvents.

Accumulation of the simulation results suggests that the aggregate microstructures have a remarkable effect on the distribution of the free end and inner blocks of the backbone. The backbone blocks can segregate according to the length of the backbone blocks between τ_{i-1} and τ_i $(1 \leq i \leq m + 1)$ in the microstructures, such as circle-like micelles assembled by graft copolymers with a hydrophobic backbone (Figure 4) and vesicles assembled by graft copolymers with a hydrophilic backbone (Figure 9). The shorter blocks localize along the interface, whereas the longer blocks are predominately concentrated in the region rich in backbone blocks. However, for the large compound micelles (Figures 6 and 10) and vesicles aggregated by graft copolymers with a hydrophobic backbone (Figure 5), the free end and inner blocks are not separated, and they are uniformly mixed in the clusters.

Finally, we wish to emphasize that, although our simulation results are in agreement with available experimental observations, there are also some drawbacks in the simulations due to neglect of thermal fluctuations in the formalism of mean-field theory. The observed aggregate morphologies of the amphiphilic copolymers in dilute solution are sensitive to the amplitude of initial density fluctuation,[44] possibly corresponding to different experimental preparation conditions, such as the concentration and quenching temperature.[59−61] Some morphologies may not correspond to the lowest free energy, and the systems can be trapped in the metastable states. These states should depend on the pathway of the system on the free energy landscape, which is governed by the initial calculation condition. Fortunately, there are some promising approaches to discern the equilibrium micelles. One approach is to calculate the free energy of candidate micelles (using SCFT/brush theories) and compare them to determine the equilibrium micelle concentrations.[62] The other method is the field-theoretic simulations,[26,43] which can numerically sample the functional integrals in a complete model that are relevant to polymer structures and thermodynamic properties. Such simulations have been used to elucidate the effects of fluctuations on order−disorder and order−order phase transitions of block copolymers,[41] as well as facilitate the studies of phases, such as polymeric bicontinuous microemulsions.[31]

Conclusions

We have investigated the aggregate morphologies of graft copolymers in dilute solution by using the two-dimensional self-consistent field theory. Two kinds of graft copolymers were discussed in the article: the backbone is hydrophobic and the grafts are hydrophilic or the backbone is hydrophilic and the grafts are hydrophobic. The graft copolymers can self-assemble to a variety of microstructures, such as circle-like micelles, line-like micelles, large compound micelles, and vesicles, depending on the architectural parameters and the interaction parameter between the graft blocks and solvents. By varying the position of the first graft point τ_1 and the number of branches m, the aggregate morphology stability regions of graft copolymers are constructed. It is found that the architectural parameters play a profound role in the complex microstructure formation. Meanwhile, the interaction between the graft blocks and solvents also has an effect on the self-assembly behavior of graft copolymers. The distributions of the free end and inner blocks of the backbone are found to be dependent on the formed microstructures. The free end and inner blocks of the backbone can segregate and localize in different parts of the aggregates depending on their length. On the other hand, the free end and inner blocks can also not be separated and be uniformly mixed in the clusters.

Acknowledgment. This work was supported by National Natural Science Foundation of China (50673026 and 20574018). Supports from Doctoral Foundation of Education Ministry of China (Grant No. 20050251008), Program for New Century Excellent Talents in University in China (NCET-04-0410), and Project of Science and Technology Commission of Shanghai Municipality (05DJ14005, 06SU07002, and 0652nm021) are also appreciated. The authors are also very grateful to the anonymous reviewers for their comments and suggestions, which resulted in an improvement of the paper.

References and Notes

(1) Hadjichristidis, N.; Pispas, S.; Floudas, G. A. *Block Copolymers: Synthetic Strategies, Physical Properties, and Applications*; John Wiley & Sons: New York, 2003.

(2) Allen, C.; Maysinger, D.; Eisenberg, A. *Colloids Surf. B* **1999**, *16*, 3.

(3) Riess, G. *Prog. Polym. Sci.* **2003**, *28*, 1107.

(4) Hadjichristidis, N.; Iatrou, H.; Pitsikalis, M.; Pispas, S.; Avgeropoulos, A. *Prog. Polym. Sci.* **2005**, *30*, 725.

(5) Bohrisch, J.; Eisenbach, C. D.; Jaeger, W.; Mori, H.; Müller, A. H. E.; Rehahn, M.; Schaller, C.; Traser, S.; Wittmeyer, P. *Adv. Polym. Sci.* **2004**, *165*, 1.

(6) Förster, S.; Abetz, V.; Müller, A. H. E. *Adv. Polym. Sci.* **2004**, *166*, 173.

(7) Iatrou, H.; Willner, L.; Hadjichristidis, N.; Halperin, A.; Richter, D. *Macromolecules* **1996**, *29*, 581.

(8) Tsitsilianis, C.; Papanagopoulos, D.; Lutz, P. *Polymer* **1995**, *36*, 3745.

(9) Ramzi, A.; Prager, M.; Richter, D.; Efstratiadis, V.; Hadjichristidis, N.; Young, R. N.; Allgaier, J. B. *Macromolecules* **1997**, *30*, 7171.

(10) Pispas, S.; Poulos, Y.; Hadjichristidis, N. *Macromolecules* **1998**, *31*, 4177.

(11) Pispas, S.; Hadjichristidis, N.; Potemkin, I.; Khokhlov, A. *Macromolecules* **2000**, *33*, 1741.

(12) Sotiriou, K.; Nannou, A.; Velis, G.; Pispas, S. *Macromolecules* **2002**, *35*, 4106.

(13) Yoo, M.; Heise, A.; Hedrick, J. L.; Miller, R. D.; Frank, C. W. *Macromolecules* **2003**, *36*, 268.

(14) Lele, B. S.; Leroux, J.-C. *Polymer* **2002**, *43*, 5595.

(15) Mountrichas, G.; Mpiri, M.; Pispas, S. *Macromolecules* **2005**, *38*, 940.
(16) Pispas, S.; Hadjichristidis, N.; Mays, J. W. *Macromolecules* **1996**, *29*, 7378.
(17) Virtanen, J.; Tenhu, H. *Macromolecules* **2000**, *33*, 5970.
(18) Virtanen, J.; Baron, C.; Tenhu, H. *Macromolecules* **2000**, *33*, 336.
(19) Breitenkamp, K.; Emrick, T. *J. Am. Chem. Soc.* **2003**, *125*, 12070.
(20) Iwasaki, Y.; Akiyoshi, K. *Macromolecules* **2004**, *37*, 7637.
(21) Tang, D.; Lin, J.; Lin, S.; Zhang, S.; Chen, T.; Tian, X. *Macromol. Rapid Commun.* **2004**, *25*, 1241.
(22) Sunintaboon, P.; Ho, K. M.; Li, P.; Cheng, S. Z. D; Harris, F. W. *J. Am. Chem. Soc.* **2006**, *128*, 2168.
(23) Borisov, O. V.; Zhulina, E. B. *Macromolecules* **2005**, *38*, 2506.
(24) Kim, K. H.; Kim, S. H.; Huh, J.; Jo, W. H. *J. Chem. Phys.* **2003**, *119*, 5705.
(25) Matsen, M. W.; Schick. M. *Phys. Rev. Lett.* **1994**, *72*, 2660.
(26) Drolet, F.; Fredrickson, G. H. *Phys. Rev. Lett.* **1999**, *83*, 4317.
(27) Matsen, M. W. *J. Chem. Phys.* **2000**, *113*, 5539.
(28) Matsen, M. W.; Bates, F, S. *Macromolecules* **1996**, *29*, 1091.
(29) Matsen, M. W. *Phys. Rev. Lett.* **1995**, *74*, 4225.
(30) Matsen, M. W. *Macromolecules* **1995**, *28*, 5765.
(31) Duchs, D.; Ganesan, V.; Fredrickson, G. H.; Schmid, F. *Macromolecules* **2003**, *36*, 9237.
(32) Matsen, M. W.; Barrett, C. *J. Chem. Phys.* **1998**, *109*, 4108.
(33) Pryamitsyn, V.; Ganesan, V. *J. Chem. Phys.* **2004**, *120*, 5824.
(34) Thompson, R. B.; Ginzburg, V. V.; Matsen, M. W.; Balazs, A. C. *Macromolecules* **2002**, *35*, 1060.
(35) Reister, E.; Fredrickson, G. H. *Macromolecules* **2004**, *37*, 4718.
(36) Reister, E.; Fredrickson, G. H. *J. Chem. Phys.* **2005**, *123*, 214903.
(37) Patel, D. M.; Fredrickson, G. H. *Phys. Rev. E* **2003**, *68*, 051802.
(38) Tang, P.; Qiu, F.; Zhang, H.; Yang, Y. *J. Phys. Chem. B* **2004**, *108*, 8434.
(39) Grason, G. M.; Kamien, R. D. *Phys. Rev. E* **2005**, *71*, 051801.
(40) Ye, X.; Shi, T.; Lu, Z.; Zhang, C.; Sun, Z.; An, L. *Macromolecules* **2005**, *38*, 8853.
(41) Ganesan, V.; Fredrickson, G. H. *Europhys. Lett.* **2001**, *55*, 814.
(42) Drolet, F.; Fredrickson, G. H. *Macromolecules* **2001**, *34*, 5317.
(43) Fredrickson, G. H.; Ganesan, V.; Drolet, F. *Macromolecules* **2002**, *35*, 16.
(44) He, X.; Liang, H.; Huang, L.; Pan, C. *J. Phys. Chem. B* **2004**, *108*, 1731.
(45) Jiang, Y.; Chen, T.; Ye, F.; Liang, H.; Shi, A.-C. *Macromolecules* **2005**, *38*, 6710.
(46) Wang, R.; Tang, P.; Qiu, F.; Yang, Y. *J. Phys. Chem. B* **2005**, *109*, 17120.
(47) Li, X.; Tang, P.; Qiu, F.; Zhang, H.; Yang, Y. *J. Phys. Chem. B* **2006**, *110*, 2024.
(48) Zhang, L.; Lin, J.; Lin, S. *J. Phys. Chem. B* **2007**, *111*, 351.
(49) Tzeremes, G.; Rasmussen, K. Ø.; Lookman, T.; Saxena, A. *Phys. Rev. E* **2002**, *65*, 041806.
(50) Rasmussen, K. Ø.; Kalosakas, G. *J. Polym. Sci., Part B: Polym. Phys.* **2002**, *40*, 1777.
(51) Frigo, M.; Johnson, S. G. *The Fast Fourier Transform in the West 2.1.3*; MIT: Cambridge, MA, 2000; http://www.fftw.org.
(52) Eyert, V. *J. Comput. Phys.* **1996**, *124*, 271.
(53) Bohbot-Raviv, Y.; Wang, Z. *Phys. Rev. Lett.* **2000**, *85*, 3428.
(54) de Gennes, P. G. *Scaling Concepts in Polymer Physics*; Cornell University Press: Ithaca, NY, 1979.
(55) Lee, H. J.; Yang, S. R.; An, E. J.; Kim, J.-D. *Macromolecules* **2006**, *39*, 4938.
(56) Haluska, C. K.; Gód, W. T.; Döbereiner, H.-G; Förster, S.; Gompper, G. *Phys. Rev. Lett.* **2002**, *89*, 238302.
(57) Antonietti, M.; Förster, S. *Adv. Mater.* **2003**, *15*, 1323.
(58) Zhang, J.; Qiu, L.; Jin, Y.; Zhu, K. *Macromolecules* **2006**, *39*, 451.
(59) Zhang, L.; Eisenberg, A. *Science* **1995**, *268*, 1728.
(60) Zhang, L.; Yu, K.; Eisenberg, A. *Science* **1996**, *272*, 1777.
(61) Zhang, L.; Eisenberg, A. *Macromolecules* **1996**, *29*, 8805.
(62) Duque, D. *J. Chem. Phys.* **2003**, *119*, 5701.